



Full Text View

[Volume 28, Issue 2 \(February 1998\)](#)

Journal of Physical Oceanography

Article: pp. 250–265 | [Abstract](#) | [PDF \(280K\)](#)

Eddy-Induced Heat Transport in a Coupled Ocean–Atmospheric Anomaly Model

Sybren S. Drijfhout and Fred H. Walsteijn

Royal Netherlands Meteorological Institute, De Bilt, the Netherlands

(Manuscript received January 22, 1997, in final form June 5, 1997)

DOI: 10.1175/1520-0485(1998)028<0250:EIHTIA>2.0.CO;2

ABSTRACT

The midlatitude meridional heat transport in the ocean can be partitioned into a transport by the mean flow and an eddy transport. This heat transport has been studied in several ocean-only models. Surprisingly, it was found that eddy-resolving and coarse-resolution models have similar total heat transport. This is caused by a compensation mechanism in which poleward eddy transport is counterbalanced by an eddy-induced meridional circulation. Recently it was shown that this compensation depends on details of the atmospheric forcing and, in fact, only occurs for weak thermal coupling, where thermal coupling is defined as the rate of change of the surface heat flux with respect to the sea surface temperature (SST). The thermal coupling varies with the spatial scale of the SST anomaly. To study the actual strength of this coupling on the eddy length scale the authors have coupled an isopycnic ocean model (with embedded mixed layer) to an atmospheric anomaly model. By comparing coarse-resolution and eddy-resolving simulations it is found that 1) the thermal coupling is strong on the eddy length scale and 2) the aforementioned compensation does not occur. Consequences for the temperature boundary condition in ocean-only models, the Gent and McWilliams eddy parameterization, and climate modeling are discussed.

1. Introduction

From the difference between absorbed and outgoing radiation at the top of the atmosphere one can estimate the meridional heat transport needed to maintain balance in the planetary heat budget. The atmosphere and ocean are then found to be equally important, albeit with different latitudinal distributions ([Carissimo et al. 1985](#)). In model calculations the heat transport in the ocean is dominated by the large-scale circulation ([McCann et al. 1994](#)).

Table of Contents:

- [Introduction](#)
- [Description of the numerical](#)
- [The modeled circulation](#)
- [Eddy-mean flow](#)
- [Discussion and conclusions](#)
- [REFERENCES](#)
- [TABLES](#)
- [FIGURES](#)

Options:

- [Create Reference](#)
- [Email this Article](#)
- [Add to MyArchive](#)
- [Search AMS Glossary](#)

Search CrossRef for:

- [Articles Citing This Article](#)

Search Google Scholar for:

- [Sybren S. Drijfhout](#)
- [Fred H. Walsteijn](#)

Locally the heat transport by mesoscale eddies can be of equal magnitude, but globally it is of less importance compared to the transport by the mean circulation.

This is consistent with the fact that low-resolution OGCMs are capable of simulating the ocean circulation with both a realistic integrated meridional heat transport and a realistic distribution of water masses (e.g., [England 1993](#); [Maier-Reimer et al. 1993](#); [Drijfhout et al. 1996](#)). However, when such low-resolution ocean models are coupled to an atmospheric model, the coupled models either exhibit climate drift or they need flux correction to avoid the climate drift. It is probable that this mismatch in fluxes between ocean and atmosphere is at least partly due to errors in the ocean model that are related to the parameterization of processes acting on unresolved scales.

Poleward heat transport by the large-scale ocean circulation is mainly accomplished by two different mechanisms. The first is the thermohaline-driven deep overturning; the second mechanism is the wind-driven gyre circulation and associated shallow wind-driven overturning. Both mechanisms are partly determined by small(er) scale processes: mesoscale eddies and convective chimneys. Within the last decade the contribution of these small-scale processes to the global ocean circulation and its heat budget has been widely appreciated. In many ocean models the Gent and McWilliams parameterization of eddy-induced tracer transport ([Gent and McWilliams 1990](#); [Gent et al. 1995](#)) has been implemented. It has been demonstrated that the effect on the global distribution of tracer, the convective activity, and the surface heat flux are large (e.g., [Danabasoglu and McWilliams 1995](#); [Hirst and McDougall 1996](#)).

When one considers the effect of the eddies on the heat budget in the ocean compared to the heat budget in a coarse-resolution model, both the eddy heat transport and the eddy-induced change in heat transport by the mean flow have to be taken into account. In general, in coarse-resolution models the thermohaline-driven deep overturning is tuned such that a realistic global conveyor belt is recovered (e.g., [Maier-Reimer et al. 1993](#)). At present, it is not known whether this circulation would be changed by the eddies, due to its long timescale and the associated computational burden when resolving the eddies. More studies have been devoted to the effect of eddies on the heat transport by the wind-driven gyre and the wind-driven overturning. It has often been observed that the sum of the heat transport by the eddies, the heat transport implied by the explicit diffusion, and the heat transport by the large-scale wind-driven circulation is almost independent of the resolution ([Cox 1985](#); [Bryan 1986](#)). [Bryan \(1986, 1991\)](#) proposed that the inherent compensation between eddy transport and eddy-induced change in transport by the mean flow would be the result of a nonacceleration theorem connected to the Eliassen–Palm theory ([Andrews et al. 1987](#)).

This assumption has been investigated by [Drijfhout \(1994a\)](#). In that paper it was shown that the eddies induce a change in the wind-driven overturning by altering the east–west cross-basin pressure gradient at midlatitudes. Within the midlatitude jet, the eddies transport heat poleward and westward. The heating of the western part of the basin is associated with the formation of a standing wave within the midlatitude jet that displaces the front between warm water and cold water at the (cool) western side of the basin farther northward. As a result, a warm anomaly develops there that reduces the cross-basin temperature gradient.

In [Drijfhout \(1994b\)](#) it was further shown that a compensation between the eddy heat transport and the eddy-induced change in heat transport by the wind-driven overturning only exists when the diabatic forcing is weak. It was concluded that this compensation depends on the way the atmospheric forcing is parameterized in ocean-only models. In general, this forcing consists of relaxing the sea surface temperature (SST) to a prescribed apparent air temperature with a fixed time constant. This results in a constant rate of change of the surface heat flux with respect to the SST. Within the coupled system the change in heat flux will depend on the wind and on the subtle processes by which an anomalous air temperature is formed in conjunction with the SST anomaly. The air temperature anomaly acts to reduce the air–sea temperature difference that reduces the sensitivity of heat flux to the SST anomaly, that is, the thermal coupling. The effectiveness of this process depends on the spatial scale of the SST anomaly (e.g., [Bretherton 1982](#); [Rahmstorf and Willebrand 1995](#)). In ocean-only models the thermal coupling is tuned to match typical SST–air temperature anomalies of a scale of 1000 km. At smaller scales the air temperature anomaly associated with an SST anomaly should become smaller and the thermal coupling should become stronger.

To investigate the effect of the thermal coupling on the role of the eddies in the ocean heat transport [Drijfhout \(1994b\)](#) compared the heat budget between a coarse-resolution and eddy-resolving model for a whole range of SST relaxation timescales. When the thermal coupling was weak, the mesoscale SST anomalies remained almost unchanged between the event of eddy formation and the reabsorption of the eddy by the mean flow. In that case the compensation between eddy heat transport and eddy-induced change in mean heat transport arises. When the thermal coupling was strong, cancellation between the indirect cell associated with the eddy heat transport and the eddy-induced change in the wind-driven overturning cell ceased to exist. A tight recirculation, southwest of the midlatitude jet, was established. This recirculation advects cold water from the northeast to the western side of the basin, which offsets the westward heat transport of the eddies within the midlatitude jet. The standing wave was still present, but near the western coast slope water spreaded farther to the south. The eddies induced a significant change in total heat transport.

The question whether eddies modify the total poleward heat transport is also important for the parameterization of eddy

transports. A recent parameterization (Gent and McWilliams 1990; Gent et al. 1995) expresses the effect of eddies under adiabatic circumstances as a downgradient thickness diffusion. When the diabatic forcing is weak, thickness diffusion does not match the eddy thickness (heat) transport very well within the midlatitude jet (Drijfhout 1994a), and an eddy-induced change in transport by the mean flow arises. In that case eddy transports give rise to a much sharper and larger peak within the midlatitude jet than can be obtained with a diffusion parameterization. One probably has to evoke a negative eddy viscosity for momentum together with thickness diffusion to mimic the eddy transports.

When the diabatic forcing is strong, a diffusion term parameterizes the eddy transport better (the peak gets broader, its maximum value smaller). In that case, however, the eddy-induced change in total heat transport obtains the same magnitude as the eddy transport itself. This suggests that the Gent and McWilliams parameterization could be improved when accounting for the effect of eddies on the heat forcing; see also Tandon and Garrett (1996) for a discussion on the effects of diabatic processes on the Gent and McWilliams parameterization.

So, the role that eddies play in the poleward heat transport depends on the strength of the diabatic forcing of the eddy scale, which is prescribed in ocean-only models. This leaves two questions: 1) what is the strength of the diabatic forcing of the eddy-scale and 2) what is the actual role of the eddies in the ocean's heat transport? To answer these questions one would ideally use observations. To this end, however, one would need a multiyear synoptic dataset of SST and air temperature or air-sea heat flux, on at least a 30-km scale of a region where the eddy kinetic energy is large. At present such a dataset is not feasible, and we will use an eddy-resolving isopycnic ocean model with explicit mixed layer physics coupled to an atmospheric anomaly model (Luksch and von Storch 1992; Luksch 1996) to address the aforementioned questions. The atmospheric anomaly model consists of a prognostic equation for anomalous air temperature advected by the mean wind and forced by an anomalous heat flux. The anomalous heat flux also forces the ocean (SST) and is proportional to the difference between anomalous SST and anomalous air temperature. In this model, SST anomalies feed back to the thermal forcing, and the effective damping timescale (coupling strength) for SST anomalies is determined by the mean atmospheric circulation and the spatial scale of the SST anomaly itself.

The outline of the paper is as follows. A description of the ocean and atmosphere model is given in [section 2](#). A comparison of mean flow fields with and without eddies is given in [section 3](#). The associated eddy-mean flow interaction is discussed in [section 4](#). In [section 5](#) the results are interpreted and we present our conclusions.

2. Description of the numerical model

In this section a short description is given of the numerical model. The model consists of an isopycnic ocean model, a mixed layer model, and an atmospheric anomaly model. The model domain has been outlined in [Drijfhout \(1994a\)](#). It consists of a closed basin that describes an idealized North Atlantic midlatitude jet and subtropical gyre.

a. Ocean model

The ocean model consists of a five-layer primitive equation isopycnic model as described by [Bleck and Boudra \(1986\)](#) and [Bleck and Smith \(1990\)](#). Two versions with different bottom topography have been used. In Mod 1 the bottom topography mimics the continental slope beneath the western boundary current and an idealization of the Mid-Atlantic Ridge at the eastern side of the basin. The maximum depth is 4000 m. Mod 2 has a flat bottom at a depth of 4000 m. A linearized equation of state has been used and the salinity is kept constant. The five isopycnic layers have densities corresponding to temperatures of 2°C, 8°C, 14°C, 20°C, and 26°C. The associated reduced gravity at the interfaces below the mixed layer is $g' = 1.2 \times 10^{-2} \text{ m s}^{-2}$ for each layer.

The equations for the ocean model are discussed in [Drijfhout \(1994a,b\)](#). The model differences from those earlier studies are the inclusion of a mixed layer model, a diapycnal diffusion term, and the coupling to an atmospheric anomaly model. The diapycnal diffusion term enters the equation for layer thickness h ;

$$\frac{\partial h}{\partial t} + \nabla \cdot \mathbf{U} = -B_T \nabla^4 h + \mu \frac{\partial^2 h}{\partial s^2}, \quad (2.1)$$

where s is the vertical coordinate. The diffusion coefficient μ is chosen to be $10^{-4} \text{ m}^2 \text{ s}^{-1}$. There still is a discrepancy between the value of the diapycnal diffusion as inferred from large-scale models, $O(10^{-4} \text{ m}^2 \text{ s}^{-1})$, and as inferred from microstructure measurements, $O(10^{-5} \text{ m}^2 \text{ s}^{-1})$; see [Davis \(1994\)](#). Probably, the reason is that diapycnic mixing is much larger near boundaries (shelf slopes) and above rough bottom topography (midocean ridges) than in the ocean's interior ([Polzin et al. 1997](#)). As an explicit parameterization of boundary and slope mixing still is lacking, these processes are included in ocean models by enhanced interior mixing. We note that in the present model diapycnic diffusion is only important for layers that are weakly ventilated, that is, the deep ocean. In the upper ocean the effect of diapycnic mixing is overwhelmed by water exchange with the mixed layer. Since eddy-induced changes of the mean flow are mainly restricted

to the upper ocean, for the results are insensitive to the value of the diapycnal diffusion coefficient as long as it is less than $O(10^{-2} \text{ m}^2 \text{ s}^{-1})$. The implementation of the diapycnic diffusion is according to [Huang and Bryan \(1987\)](#).

b. Mixed layer physics

The mixed layer is forced by wind stress and a heat flux. For the uncoupled runs we assume that the timescale for SST anomalies is proportional to the depth of the mixed layer. For a mixed layer depth of 50 m we choose this timescale to be 10 days. The heat flux is obtained by relaxing the SST to a zonally averaged temperature with a restoring time constant that is equal to 10 days times the mixed layer depth divided by 50 m. This heat flux will be used as a climatological mean forcing in the later coupled runs. The SST restoring timescale of ten days only affects the mean state of the coupled runs but not the variability and the role of eddies in those runs. The wind stress profile has an idealized sinusoidal form that results in a 2½ gyre circulation. Both the wind stress and heat forcing resolve the seasonal cycle. The amplitude varies sinusoidally between the extremes in the winter and summer. The extremes are indicated in [Fig. 1](#).

The mixed layer model is an integral model that uses an energy balance to calculate the mixed layer depth ([Bleck et al. 1989](#)). The turbulent kinetic energy input is calculated every time step. The model entrains or detraines water into, or out of, the mixed layer according to the net energy generation by the forcing. At each time step the net energy generation is, according to [Bleck et al. \(1989\)](#),

$$E\Delta t = \left[(2/h)mu^{*3} + \frac{B_0 - |B_0|}{2} + n\frac{B_0 + |B_0|}{2} \right] \Delta t, \quad (2.2)$$

where E denotes the total energy, B_0 is the buoyancy flux at the surface, u^* is the friction velocity, and n and m are tuning parameters chosen to be 0.4 and 2.5 respectively. The energy input by the wind has been made a function of the ratio of the mixed layer depth to the Ekman depth. We have chosen m twice as large as in [Bleck et al. \(1989\)](#), as we use monthly averaged winds; see [Sterl and Kattenberg \(1994\)](#) for a discussion.

When $E\Delta t$ is positive, entrainment occurs. The subsequent increased mixed layer depth h implies a larger potential energy for the fluid column under consideration. The increase in h is calculated by equating $E\Delta t$ to the associated increase in potential energy; see [Bleck et al. \(1989\)](#) for more details. When $E\Delta t$ is negative, detrainment occurs. In that case, the mixed layer detraines to the Monin–Obukhov depth or to the Ekman depth, depending on which of the two is the largest. In general, the detrained mixed layer water is warmer (lighter) than the layer into which it is detrained, which cannot be represented within an isopycnic model. The detrained water must be cooled (made denser), and to conserve heat or mass the remaining mixed layer water is heated. To prevent excessive heating of the mixed layer Bleck et al. proposed to limit the amount of water detrained within one time step. In that case, the new mixed layer depth is controlled by this limiter and falls in between the old depth and the Ekman, or Monin–Obukhov, depth.

The equation for the sea surface temperature reads

$$\frac{\partial T}{\partial t} + \nabla \cdot uT = -B_T \nabla^4 T + Q/\rho c_p h, \quad (2.3)$$

where T is the SST, Q is the heat flux due to the temperature restoring condition, ρ is the density of seawater, and c_p is the specific heat of water. To avoid very thin mixed layers becoming excessively hot, Q is distributed over the upper 20 m when the mixed layer becomes smaller than 20 m. In that case, a part of the heat is used for a mass exchange between the two uppermost subsurface layers.

Before the mixed layer module is activated within the model, convective adjustment is applied to ensure a stable stratification. For more details and a description of the effect of the mixed layer on the model solution we refer to [Hazeleger and Drijfhout \(1998\)](#).

c. The atmospheric anomaly model

First, the ocean only model is spun up with the forcing described above. When the model has reached a cyclostationary state the equivalent heat flux is diagnosed from the temperature restoring condition. Thereafter, a flux condition for temperature is used consisting of the climatological mean flux plus an anomalous heat flux. The latter is coupled to SST anomalies and air temperature anomalies. The SST anomalies are calculated in a straightforward manner by applying the model equation for temperature and calculating the difference between the actual SST and the climatological mean from the spinup run. For the anomalous air temperature a prognostic equation is used:

$$\frac{\partial T_{\text{an}}^{\text{A}}}{\partial t} + \nabla \cdot \mathbf{u}^{\text{A}} T_{\text{an}}^{\text{A}} = Q_{\text{an}} / \rho^{\text{A}} c_p^{\text{A}} H + Q_{\text{D}} / \rho^{\text{A}} c_p^{\text{A}} H, \quad (2.4)$$

where the superscript ^A refers to air, the subscript _{an} refers to anomalous: T_{an}^{A} is the anomalous air temperature and Q_{an} is the anomalous heat flux; H is the height of the atmospheric model layer, chosen to be 1 km, the typical boundary-layer height directly affected by SST anomalies. The anomalous air temperature is advected by the mean wind, which is derived from the wind stress pattern used to force the ocean model. Here Q_{D} is a damping term to parameterize unresolved processes, such as baroclinic processes, turbulence, and cloud/radiation processes. This damping term consists of damping the anomalous air temperature with a timescale of ten days, a typical timescale for atmospheric cyclones,

$$Q_{\text{D}} = -\rho^{\text{A}} c_p^{\text{A}} H T_{\text{an}}^{\text{A}} / (10 \text{ days}). \quad (2.5)$$

Finally, the anomalous heat flux Q_{an} is calculated from the difference between the anomalous air temperature and the SST anomaly:

$$Q_{\text{an}} = \rho^{\text{A}} c_p^{\text{A}} c_H \mathcal{E} \{ |\mathbf{u}^{\text{A}}|^2 + 4\sigma_u^2 \}^{1/2} (T_{\text{an}}^{\text{A}} - \text{SST}_{\text{an}}), \quad (2.6)$$

where c_H is the bulk transfer coefficient for sensible heat, $c_H = 1.3 \times 10^{-3}$; \mathcal{E} is the ratio between total heat flux (sensible plus latent) to the sensible heat flux (\mathcal{E} equals one plus the inverse of the Bowen ratio). We have chosen $\mathcal{E} = 4$, which implies a typical value for the Bowen ratio of 1/3 (Stull 1989). Here σ_u is the standard deviation of the scalar wind speed, a parameterization of the variability of the wind. It is chosen to be 2.5–3.5 m s⁻¹ in summer, linearly increasing from the southern to the northern boundary of the model; in winter it is 2.5–4.5 m s⁻¹. These values are in accordance with Wright (1988).

The damping term in Eq. (2.4) plays the same role as the horizontal diffusion in the equation for SST: it damps the small-scale noise. In general, the damping term is two orders of magnitude smaller than the anomalous heat flux forcing and the advective term in Eq. (2.4). As long as the damping timescale is not chosen to be in the order of an hour or less, the results are not very sensitive to the magnitude of this term. For more details of the atmospheric anomaly model we refer to Luksch and Storch (1992) and Luksch (1996).

In one experiment the atmospheric model is extended to also include an anomalous atmospheric wind, which is connected to the atmospheric anomalous air temperature through the thermal wind relation. The assumption has been made that above the scale height H the anomalous air temperature is zero.

3. The modeled circulation

a. Experimental design

The spinup (1000 yr) of the model was done with a coarse resolution, that is, 148 km (about 4/3° × 4/3°). Laplacian friction was used, the viscosity parameter A_M was 10⁴ m² s⁻¹, and the diffusivity parameter A_T was 1.5 × 10³ m² s⁻¹. In the uncoupled runs, the thermal forcing consisted of relaxing SST to prescribed values with a 10-day time constant for a mixed layer depth of 50 m, otherwise proportional to the mixed layer depth. A similar coupling strength, 240 W m⁻² K⁻¹, has been used by Luksch and Storch (1992) in their uncoupled experiment. This coupling strength should be thought of as a maximum value that occurs when no atmospheric feedbacks are operative. When the model is coupled, atmospheric feedbacks are capable of reducing the effective coupling strength. In that case the heat flux climatology is diagnosed from the spinup with the strong coupling and heat flux anomalies are calculated with a bulk formula. The latter determine the coupling strength in the coupled experiments.

After the first 1000 years of spinup the model resolution has been decreased to 74 km. With the same diffusivity and a viscosity parameter of 3 × 10³ m² s⁻¹ the model reached again a cyclostationary state within an extended spinup of 100 yr. The climatology for the low-resolution eddyless experiments has been taken from the last 25 years of this extended spinup. Four experiments have been carried out (see Table 1). The first three experiments have been run with Mod 1, the model version with bottom topography.



Experiment 1 is the standard experiment. It consists of the isopycnic model coupled to the atmospheric anomaly model. Experiment 2 consists of the uncoupled ocean model only. This experiment is designed to test the effect of atmospheric


feedbacks on the air–sea heat flux. Experiment 3 consists of the same coupled model as used in experiment 1, but now the atmospheric model is extended to account for anomalous winds related to the anomalous air temperature by the thermal wind relation. This experiment is designed to test the influence of nonlinear feedbacks on the air–sea heat flux. Experiment 4 consists of the same configuration as the standard experiment, experiment 1, but now the ocean model is the flat-bottom version of Mod 2. The separation latitude of the midlatitude jet and the associated standing wave appears to be rather sensitive to details of the bottom topography. Experiment 4 is designed to test the robustness of the conclusions obtained with Mod 1 for changes in the structure and climatology of the midlatitude jet.

The four experiments mentioned above can be separated into two parts: One part consists of the experiments i^a , which are the low-resolution runs without eddies. The second part consists of the experiments i^b , which are the high-resolution runs that resolve mesoscale eddies. In the latter experiments the grid size was further reduced to 37 km. From [Drijfhout \(1994a\)](#) we know that with the present forcing and configuration a further reduction in resolution results in an increase in the average level of eddy kinetic and potential energy but no qualitative changes occur between eddy-resolving experiments of 37-km and 18.5-km resolution.

In the experiments i^b , biharmonic friction has been applied. The diffusivity parameter was $6 \times 10^{11} \text{ m}^4 \text{ s}^{-1}$, the viscosity was chosen to depend on the deformation rate ([Bleck and Boudra 1981](#)) with a minimum value of $10^{11} \text{ m}^4 \text{ s}^{-1}$. The eddy-resolving experiments have been run for 15 years. The climatology for these runs was taken from the last 5 years.

b. Experiment 1: The standard experiment

First, we discuss the features common to all four experiments. This discussion will focus on the results of experiment 1 ([Table 1](#) ) . [Figure 2](#)  shows the barotropic streamfunction for experiments 1^a and 1^b . The imposed wind forcing drives a $2\frac{1}{2}$ gyre circulation. The mass transport in the subtropical gyre is enhanced by a factor of 2 in experiment 1^b due to a downward transport of momentum by the eddies. It is also evident that the western boundary current is narrower when eddies are resolved. In this experiment the midlatitude jet develops a standing wave pattern, as in [Drijfhout \(1994a,b\)](#). The structure of the standing wave pattern, however, is different and the associated overshoot in separation of the midlatitude jet is much larger. It appears that this overshoot in the eddy-resolving experiment depends, among others, on the topography. This feature will be discussed in more detail in [section 3e](#).

The mixed layer depth has maximum values in the north ([Fig. 3](#) ) , where the coldest air resides. A second maximum is found at the southern flank of the midlatitude jet, some 300 km from the western boundary. Here, cooling of SST exhibits a second maximum and the model counterpart of mode water is formed ([Hazeleger and Drijfhout 1996](#)). Beneath the mixed layer, the 26°C isopycnic layer is limited to the southeast of the model domain. The outcropping patterns (not shown) for the 14°C , 20°C , and 26°C layers indicate a rather strong thermal driving. The outcropping line and height contours roughly follow latitudes that coincide with the thermal forcing pattern; they are much less influenced by the wind-driven circulation. This feature is associated with the regime of strong thermal forcing. We can predict from the results of [Drijfhout \(1994b\)](#) that the eddies will induce changes in the total heat transport and the heat forcing in this model.

The meridional heat transport can be evaluated by integrating the (zonally and vertically averaged) heat equation from the southern boundary to a latitude y_0 . We then obtain the meridional heat transport at latitude y_0 , balanced by the integrals of the surface flux, horizontal and vertical diffusion, convection, and tendency (heat storage). A more detailed description of this calculation is given in [Drijfhout \(1994a\)](#).

For the experiments *a*, without eddies, the heat equation can be written in steady state as

$$\nabla \cdot (\overline{h\mathbf{u}T}) = Q + D, (3.1)$$

where D denotes horizontal and vertical diffusion, and Q denotes the heat forcing at the air–sea interface. For the experiments *b*, with eddies, the heat equation for the statistically steady state becomes

$$\nabla \cdot (\overline{h\mathbf{u}T^*} + \overline{h'\mathbf{u}'T}) = Q + \Delta Q + D^*. (3.2)$$

Now, D^* also includes the term $-\nabla \cdot [(\overline{h\mathbf{u}})'T]$, which is assumed to be small.

Heat transport compensation arises when the term $\overline{h'\mathbf{u}'T}$ is compensated by a change in the term $\overline{h\mathbf{u}T}$, so that $\nabla \cdot (\overline{h\mathbf{u}T^*} + \overline{h'\mathbf{u}'T})$ in [Eq. \(3.2\)](#) approximately equals $\nabla \cdot (\overline{h\mathbf{u}T})$ in [Eq. \(3.1\)](#). This equality is approximate, in so far as the difference between D^* and D has to be accounted for, which in general is much smaller than the difference between $\overline{h\mathbf{u}T^*}$ and $\overline{h\mathbf{u}T}$. In that case ΔQ in [Eq. \(3.2\)](#) is zero. Both the heat forcing and total heat transport remain unchanged between the experiment with, and without, eddies.

In the case that the heat transport compensation is zero, $\overline{h'u'T} = \overline{h'u'T}^*$. In that case, $\overline{h'u'T}$ induces a change in heat forcing ΔQ , apart from the difference between D^* and D , which in general is much smaller than $\overline{h'u'T}$. The eddy heat transport is associated with an eddy-induced change in total heat transport of about equal magnitude.

The heat balance for experiment 1 is illustrated in [Fig. 4](#). The integrated surface heat flux (which equals the total heat transport) differs significantly in the midlatitude jet region for the experiment with and without eddies; that is, the term ΔQ in [Eq. \(3.2\)](#) is significant. In the coupled model the forcing of the eddy scale is so strong that the eddies change significantly the zonally averaged SST and associated heat budget. Within the midlatitude jet region also the poleward eddy heat transport shows a maximum ([Fig. 5](#)). This downgradient heat transport is associated with the baroclinic instability of the jet. The eddy-induced change in total heat transport and the eddy heat transport itself are very similar and have the same magnitude: $\overline{h'u'T}$ and $\int \Delta Q \, dy$ are about equal. The maximum eddy-induced change in total heat transport, however, is displaced 4° lat northward with respect to the maximum in eddy heat transport. This point will be discussed further in [section 5](#).

c. Experiment 2 versus experiment 1: The role of coupling

In the uncoupled experiment the thermal coupling coefficient is $240 \text{ W m}^{-2} \text{ K}^{-1}$. In the coupled experiment this coefficient (γ) becomes

$$\gamma = c_H \epsilon c^w \rho^w \{ |\mathbf{u}^A|^2 + 4\sigma_u^2 \}^{1/2} (\text{SST}_{\text{an}} - T_{\text{an}}^A) / \text{SST}_{\text{an}}. \quad (3.3)$$

[Equation \(3.3\)](#) implies that, if the anomalous air temperature and anomalous SST are uncorrelated, the thermal coupling γ is equal to $21 \text{ W m}^{-2} \text{ K}^{-1}$ times the nondimensionalized average wind speed. In the coupled model, the thermal coupling will be reduced when the anomalous air temperature and SST anomalies are positively correlated. When T_{an}^A is on the average a certain percentage of SST_{an} the thermal coupling is also reduced with that certain percentage.

In experiment 1^a the average coupling coefficient is $118 \text{ W m}^{-2} \text{ K}^{-1}$; the average fraction of $T_{\text{an}}^A / \text{SST}_{\text{an}}$ is less than 10%. Variations in the thermal coupling coefficient are almost wholly determined by variations in the average absolute wind speed. In experiment 1^b the thermal coupling coefficient is almost unchanged, $115 \text{ W m}^{-2} \text{ K}^{-1}$. The spatial distribution of the thermal coupling is displayed in [Fig. 6](#). Although the average thermal coupling is reduced by a factor of 2, the differences in ocean circulation between experiments 1 and 2 are negligible. Apparently the ocean is insensitive to further changes in the thermal coupling when the coupling is already strong, that is, larger than $115 \text{ W m}^{-2} \text{ K}^{-1}$. When eddies are included the sensitivity to the ocean circulation is somewhat larger than in the case where eddies are unresolved. In experiment 1^b the heat transport in the southern part of the model is reduced compared to experiment 2^b. The maximum reduction is 15% of the maximum total heat transport ([Fig. 7](#)). This feature is confirmed by the average anomalous air temperature and anomalous SST ([Fig. 8](#)). The southern part of the domain is warmed up with a maximum value of 0.2°C , the maximum anomalous SST is 5.0°C . The reduction in air–sea heat flux in the southern part of the domain is balanced by reduced upwelling. This results in a decrease of the southern wind-driven overturning cell by 20% and an increase of the mixed layer depth in the midlatitude jet (not shown).

The thermal coupling of $115 \text{ W m}^{-2} \text{ K}^{-1}$ in the coupled model is so strong that coupling has no impact on the eddy-induced change in total heat transport. The coupled model establishes a regime of strong thermal driving with respect to eddy–mean flow interaction. The atmospheric feedback on the air–sea heat flux is negligible on the eddy scale. These results suggest that the eddy heat transport compensation found in, for example, [Cox \(1985\)](#), [Böning and Budich \(1992\)](#), [Beckmann et al. \(1994\)](#), and [Böning et al. \(1996\)](#) might be the results of inadequate air–sea interaction [a typical value for the coupling coefficient in these models is $25\text{--}60 \text{ W m}^{-2} \text{ K}^{-1}$; [Böning et al. \(1996\)](#)].

[Bretherton \(1982\)](#) suggested that the thermal coupling coefficient for small-scale SST anomalies should be about $100 \text{ W m}^{-2} \text{ K}^{-1}$. Compared to this estimate the coupling coefficient of $115 \text{ W m}^{-2} \text{ K}^{-1}$ observed in the present coupled model is fairly realistic. [Drijfhout \(1994b\)](#) suggested that the thermal coupling at the eddy length scale would undergo a transition between a regime of weak coupling and strong coupling when the thermal coupling coefficient becomes larger than about $100 \text{ W m}^{-2} \text{ K}^{-1}$. This is confirmed with the present result. With a coupling coefficient of $115 \text{ W m}^{-2} \text{ K}^{-1}$ the thermal coupling is strong on the eddy length scale.

d. Experiment 3 versus experiment 1: The role of nonlinear feedbacks

In this experiment the atmospheric anomaly model is extended to include an anomalous wind field is diagnosed from the

anomalous air temperature by the thermal wind relation. In that case, anomalous air temperatures can also be induced by advection of air temperature through the anomalous wind. Also, the atmospheric model is now capable of transporting heat poleward. This nonlinear anomaly model, however, behaves very similarly to the linear model of experiment 1. The effective coupling coefficient is hardly changed ($114 \text{ W m}^{-2} \text{ K}^{-1}$ versus $115 \text{ W m}^{-2} \text{ K}^{-1}$ in experiment 1^b, compare [Figs. 9](#) and [6](#)). The impact on the heat transport compared to experiment 1^b is negligible. With a coupling to both a linear and a nonlinear anomaly model the atmospheric feedbacks on the air–sea heat flux are negligible on the eddy scale. The coupling coefficient can be approximated by [compare with [Eq. \(3.3\)](#)]

$$\gamma = c_H \mathcal{E} c_p^w \rho^w \{ |\mathbf{u}^A|^2 + 4\sigma_u^2 \}^{1/2}. (3.4)$$

e. Experiment 4 versus experiment 1: The role of bottom topography

In experiment 1^b the separation latitude of the midlatitude jet has shifted a large distance northward due to eddy–mean flow interactions. One might hypothesize that the large overshoot in midlatitude jet separation determines the absence of heat transport compensation in experiment 1. In [Drijfhout \(1994a,b\)](#) heat transport compensation arose through a warming of the western boundary by the eddies that lead to a reduction of the cross-basin pressure gradient and a subsequent increase of the wind-driven overturning in the midlatitudes. This increase in overturning compensated the eddy heat transport in midlatitudes when the thermal coupling is weak. In experiments 1, 2, and 3 an eddy-induced warming of the western boundary and heat transport compensation are absent. Experiment 4 is designed to test whether this absence of an eddy-induced warming of the western boundary is determined by the strong thermal coupling or whether it is an artifact associated with the overshoot in separation of the midlatitude jet.

In experiment 4^b the overshoot is almost absent ([Fig. 10](#)). In the flat-bottom experiment the eddy-induced change in heat transport is somewhat less compared to experiment 1^b, while the eddy heat transport itself is somewhat stronger. This can be understood as the effective coupling is decreased because the velocities in the subtropical gyre are larger compared to experiment 1^b, which decreases the advective timescale of SST anomalies (see [Drijfhout 1994a](#)). This decrease in effective coupling, however, is so small that the eddy-induced change in total transport is still of the same magnitude as the eddy heat transport. The lack of heat transport compensation and the strong forcing of the eddy scale is associated with the nature of the air–sea interaction. It is not associated with a spurious overshoot in separation of the midlatitude jet.

The larger velocities in the subtropical gyre in experiment 4 are associated with an increase of the eddy-induced enhancement in mass transport. The maximum mass transport in the subtropical gyre increases due to the eddies from 50 to 120 Sv in experiment 4, while in experiment 1 the increase is from 50 to 100 Sv (compare [Figs. 2](#) and [10](#)). This difference in eddy-induced enhancement in mass transport arises because in experiments 1, 2, and 3 bottom topography dissipates the eddy-driven deep circulations ([Böning 1989](#)). Moreover, in experiment 4 the eddy-driven barotropic mode is enhanced as the ocean has become deeper.

4. Eddy–mean flow interaction

Below the mixed layer, variations in density, or temperature, are equivalent to variations in the thickness between two isopycnal surfaces. An eddy heat transport is associated with an eddy transport of layer thickness, or mass. When the thermal driving is weak, the eddy transport of mass is compensated by an eddy-induced change in mass transport by the mean flow; when the thermal driving is strong, these eddy-induced overturning anomalies are either absent or rearranged in such a fashion that they no longer compensate the eddy transport of mass. In this section we focus on the eddy-induced overturning anomalies to give additional insight into the relation between eddy heat transport and eddy-induced changes in total heat transport.

a. Overturning anomalies

When the thermal forcing is weak, the eddy heat transport is compensated by an enhancement of the wind-scale overturning cells. When the thermal forcing is strong, the eddy-induced overturning anomaly is more complicated. In [Drijfhout \(1994b\)](#) it was shown that the anticlockwise overturning cell at midlatitudes intensifies, but it is displaced downward. On top of it appears a clockwise overturning cell that is connected with the subpolar overturning cell. Near the midlatitude jet these two eddy-induced anomalous overturning cells compensate each other with respect to the heat transport, and the eddy heat transport across the midlatitude jet is no longer balanced by the eddy-induced circulation.

For the standard experiment, experiment 1 (linear coupled anomaly model), both experiments 1^a and 1^b (without eddies and eddy resolving, respectively) exhibit a meridional streamfunction with three shallow overturning cells ([Fig. 11](#)). This is qualitatively similar to the stronger forcing cases in [Drijfhout \(1994b\)](#), where also a three-cell structure was found for the

meridional overturning. A fourth, much deeper, cell reflects a meridional circulation that is not associated with diapycnic motion. Likewise, as the Deacon cell in FRAM (Döös and Webb 1994), it disappears when calculating the streamfunction as a function of density instead of depth (Fig. 12). This overturning cell is associated with the subpolar gyre at the two deepest levels. The geometry of these isopycnic surfaces is so that the southward branch of the subpolar gyre is located at shallow depths near the shelf break along the coast. The northward return flow is located farther eastward at much greater depths. The circulation on these tilted isopycnic surfaces induces a meridional circulation when calculating the streamfunction as a function of depth. A deep overturning cell associated with deep-water formation is absent in the model. Although deep water is formed every year, the advective timescale of this deep water is so small that a major fraction is reentrained every winter into the deepening mixed layer.

The similarity in overturning between experiments 1^a and 1^b implies that eddy-induced overturning anomalies are weak in the coupled model, so compensation does not occur. At the same depth, however, significant eddy-induced mass transport anomalies occur within the mixed layer and, farther eastward where the mixed layer is less deep, within the isopycnic layers just below the mixed layer. These anomalies are related to the an eddy-induced change in mixed layer depth and in particular, to the eddy-induced change in east–west slope in mixed layer depth. At a constant depth level these eddy-induced mass transport anomalies disappear. The mass transport anomalies are illustrated by presenting the meridional overturning as a function of density (potential temperature) (Fig. 13). These apparent overturning anomalies are associated with a diapycnic horizontal motion within the mixed layer. They reflect an enhancement of the heat transport by the subtropical gyre where the northward branch advects warmer water than the southward branch. This eddy-induced increase in northward heat transport by the gyre is too weak for heat transport compensation to occur. It is nearly balanced by the decrease in northward heat transport by explicit diffusion when eddies are resolved. The eddy heat transport and eddy-induced change in heat transport are almost equal, but the latter peaks farther northward due to the eddy-induced change in heat transport by the gyre (see Fig. 5). This feature is robust for all four experiments.

b. Mass transport anomalies

In the case of weak thermal driving an eddy-induced overturning anomaly is related to an anomalous east–west pressure difference by geostrophy. When the mass transport equation is considered, this eddy-induced change in pressure gradient is balanced by an equivalent Eliassen–Palm flux (Drijfhout 1994a). The eddy-induced change in total mass transport is almost zero. When the thermal driving is strong, both the eddy-induced change in forcing and the eddy-induced change in total mass transport have to be considered:

$$\Delta[\bar{V}] + \Delta[\Lambda + \bar{X} - \overline{hM}_x]/f = 0, (4.1)$$

where, for an arbitrary parameter x , \bar{x} is defined as the zonal average of x , and $[x]$ as the time average, Δ is defined as the eddy-induced change in the associated mean flow quantity, V is the meridional mass transport, $V = \mathbf{v}h$; X is any nonconservative force and Λ is the mean-flow forcing by the eddies,

$$\Lambda = \{(\overline{h\mathbf{v}})'u'\}_y + \{\overline{h'M}_x'}\}, (4.2)$$

where $x' = x - \bar{x}$. Lee and Leach (1996) demonstrated that Λ can be written as a flux divergence,

$$\Lambda = \{(\overline{h\mathbf{v}})'u' - P\}_y + \{\overline{p'M}_x'}\}_s, (4.3)$$

where P is the available eddy potential energy. So, we can interpret Λ as the divergence of an Eliassen–Palm flux for time-averaged flow in an ocean basin.

The first-order balance in Eq. (4.1) is between $\Delta[\bar{V}]$ and $\Delta[\overline{hM}_x]/f$ for all four experiments. Such a geostrophic balance is typical for a closed basin. Lee and Leach (1996), for instance, found a much more important role for the Eliassen–Palm flux divergence while using a channel model. The mean flow quantities within Eq. (4.1) become much smaller when they are taken as a function of depth instead of density, consistent with the differences between eddy-induced meridional overturning anomalies as a function of depth and density. But in both cases, the first order is geostrophic.

The eddy transport of mass is much less important compared to the mean transport than the eddy transport of heat. This implies that the eddy heat transport is mainly accomplished by temperature anomalies within the mixed layer that are only weakly correlated with mixed layer depth anomalies. Due to the strong thermal coupling the lifetime for SST anomalies is so short that the mixed layer depth does not equilibrate at this timescale. Maxima and minima in the eddy transport of mass are anticorrelated with those in the Eliassen–Palm flux divergence, but typically some 50% larger.

5. Discussion and conclusions

In the GFDL and CME model the eddy heat transport is compensated by an eddy-induced change in heat transport by the mean flow (Cox 1985; Böning and Budich 1992; Beckmann et al. 1994; Böning et al. 1996). In Drijfhout (1994b) it was shown that this mechanism is only operative when the heat forcing is weak on the eddy scale. In that case, the change in the product of layer thickness and cross-basin pressure gradient is balanced by the divergence of the Eliassen–Palm flux, which results in no net change in the residual meridional circulation and total mass and heat transport. When the heat forcing is stronger, the eddy-induced change in cross-basin pressure gradient is reversed by an eddy-induced tight recirculation south of the midlatitude jet. The change in pressure gradient is no longer balanced by the Eliassen–Palm flux divergence and an eddy-induced residual circulation arises.

In the present coupled model the thermal forcing is no longer prescribed. It establishes itself in a regime of strong forcing. On the eddy length scale the effective thermal coupling coefficient becomes $115 \text{ W m}^{-2} \text{ K}^{-1}$. It should be noted that the coupling coefficient reduces when the spatial scale of the SST anomaly increases. The average thermal coupling in a T42 coupled GCM was established at $16 \text{ W m}^{-2} \text{ K}^{-1}$ (Mikolajewicz and Maier-Reimer 1994). This scale dependency of the thermal coupling was suggested before by Bretherton (1982). Rahmstorf and Willebrand (1995) parameterized the scale dependency with a constant plus diffusive transport resulting in an almost quadratic relation between thermal coupling and the inverse of the length scale. Their cutoff value was $50 \text{ W m}^{-2} \text{ K}^{-1}$ at the 400-km length scale, being the resolution of their model. With the same parameterization, a coupling coefficient of $115 \text{ W m}^{-2} \text{ K}^{-1}$ is related to a length scale of 174 km. At this scale the quadratic increase of coupling strength with the inverse of the length scale stops. For smaller scales the coupling cannot increase further because the anomalous air temperatures and anomalous SST have become decorrelated and the coupling is determined by the average wind speed only.

The strong thermal coupling at the eddy length scale implies that the eddy heat transport compensation in the CME model is an artifact of the too weak coupling on the eddy scale ($25\text{--}60 \text{ W m}^{-2} \text{ K}^{-1}$, see Böning et al. 1996). On the other hand, it is not yet clear to which extent the coupling in the present model depends on the model configuration and basin geometry and to which extent this result can be extended to more realistic ocean models. The small basin and strong circulation tend rather to underestimate the coupling strength, and the same holds for the mixed layer model, which tends to overestimate the mixed layer depth.

The mixed layer physics in the present model is still crude, but it seems likely that more sophisticated mixed layer physics (e.g., Oberhuber 1993; Large et al. 1994) would tend to decrease the overall mixed layer depth. This causes both a decrease of the eddy-induced mass transport in the mixed layer and an increase of the coupling strength. As a result, the eddy-induced change in heat transport will only become larger. An overestimation of the coupling strength could be due to the atmospheric model. First, the scale height of the response to SST anomalies could be too small. At present, however, there is no indication that this height should be larger than 1 km at midlatitudes. The small domain and purely zonal mean wind could favor the advection of eddy-scale anomalous air temperatures too much, resulting in a too weak correlation between anomalous air temperature and anomalous SST. This does not seem likely, however, as the ratio of basin scale to eddy scale is of the order of 50.

A second implication of the strong thermal coupling at the eddy length scale is that the Gent and McWilliams parameterization of the eddy-induced transport velocity (Gent and McWilliams 1990; Gent et al. 1995) should be modified to include this effect. The implication that diabatic effects modify the Gent and McWilliams parameterization was already suggested by Tandon and Garrett (1996). If the eddies induce a change in heat forcing ΔQ , the heat equation becomes

$$\frac{\partial(hT)}{\partial t} + \nabla \cdot (\bar{h} \bar{\mathbf{u}} \bar{T} + \overline{h' \mathbf{u}' T}) = Q + \Delta Q + D, \quad (5.1)$$

where D denotes horizontal and vertical diffusion, and D also includes the term $-\nabla \cdot [(\overline{h \mathbf{u}' T})]$, which is assumed to be parameterized by diffusion. In comparison with Eq. (4) in Gent et al. (1995) we have added Q and ΔQ and included possible other diffusive terms in D . The heat equation for the large-scale model can be written as

$$\frac{\partial(hT)}{\partial t} + \nabla \cdot (\mathbf{U} \bar{h} \bar{T}) = Q + D, \quad (5.2)$$

where

$$\mathbf{U} = \bar{\mathbf{u}} + (\overline{h' \mathbf{u}'})/\bar{h} - Q^* \quad (5.3)$$

and

$$Q^* = \int (\Delta Q / \bar{h} T) dx. \quad (3.4)$$

It should be noted that ΔQ is an eddy-induced flux correction term. Furthermore, Q^* and $(\overline{h'u'})$ in general have the same sign. Neglecting eddy-induced changes in heat forcing leads to an overestimation of the eddy-induced heat transport. This is illustrated in [Fig. 14](#), which shows the meridionally integrated form (see discussion of [Fig. 4](#)) of $A_T \nabla^2 \overline{hT}$, which is the diffusive parameterization of the eddy heat transport as proposed by Gent and McWilliams (A_T is $1500 \text{ m}^2 \text{ s}^{-1}$ in this experiment), $\overline{h'u'T}$, and $\overline{h'u'T} - \int \Delta Q dy$, which is the eddy heat transport minus the eddy-induced change in total heat transport. Qualitatively there is a reasonable agreement between the eddy heat transport and the diffusive parameterization. This agreement only exists in the regime of strong thermal forcing. When the thermal forcing is weak, the peak in eddy heat transport within the midlatitude jet is larger and sharper than can be modeled by diffusion. In that case, the eddy heat transport should be parameterized with larger diffusion coefficients together with a negative eddy viscosity parameterization to simulate both a large diffusive transport and a very sharp midlatitude jet. When the thermal coupling is strong, the eddy heat transport itself can be modeled by a diffusive transport. But then, also a parameterization for the eddy-induced change in heat forcing is needed.

[Figure 14](#) shows that, when the eddy-induced change in heat forcing is subtracted from the eddy heat transport, the net result does not scale very well with a thickness diffusion parameterization. The peak in the eddy-induced change in heat forcing is northward from the peak in the eddy heat transport itself (see also [Fig. 5](#)). From [Fig. 14](#) we see that

$$\overline{h'u'T} - \int \Delta Q dy$$

scales better with the spatial derivative of thickness diffusion than with the thickness diffusion itself. The peak in eddy-induced change in heat forcing is northward from the peak in eddy heat transport because warm core rings more quickly release heat to the atmosphere, as cooling induces convective mixing and an increase of the mixed layer depth. Cold core rings, in contrast, become easily isolated from the atmosphere through the formation of a warm shallow mixed layer on top. The cold anomaly is slowly mixed with the surroundings and often the cold core ring is recaptured before it has released its heat anomaly. If one does not account for the shift in location of the peak of eddy heat transport and eddy-induced change in forcing, the term $\overline{h'u'T} - \int \Delta Q dy$ implies a diffusive transport with diffusivities which are at least an order of magnitude smaller compared to $\overline{h'u'T}$ alone.

In summary, our main conclusions are, that, using an eddy-resolving isopycnic ocean model with explicit mixed layer physics and coupled to an atmospheric anomaly model, 1) the thermal coupling establishes itself in a regime of strong forcing (the average coupling coefficient is $115 \text{ W m}^{-2} \text{ K}^{-1}$ on the eddy scale) and 2) the eddies induce a change in total heat transport comparable to the eddy heat transport itself.

These results are robust for the use of different anomaly models (linear and nonlinear coupling) and different oceanic mean-flow profiles that are related to different bottom topography. It is not tested, however, to what extent these results are robust to the use of a different (less zonal) forcing profile, different ocean basin geometry, and the inclusion of more sophisticated (mixed layer) physics.

To describe the eddy heat transport in the regime of strong thermal forcing accurately, the Gent and McWilliams parameterization has to be improved to account for diabatic effects. The meridional profiles for the eddy heat transport and eddy-induced change in total heat transport have to be tested within a coupled model for a set of various basin geometries and forcing profiles to investigate how the eddy transport properties can be generalized into mean flow quantities.

Low-resolution ocean and climate models should incorporate such an improved Gent and McWilliams parameterization to account for eddy transports. The effect of eddies on the heat transport cannot be neglected when the ocean-atmosphere coupling is realistic.

Acknowledgments

This research was supported by the program VVA of the Netherlands Foundation of Scientific Research (NWO). Wilco Hazeleger, Arie Kattenberg Gerbrand Komen, and an anonymous reviewer are acknowledged for their comments on this manuscript. The calculations have been performed on the Cray-1 YMP of the ECMWF in Reading.

Andrews, D. G., J. R. Holton, and C. B. Leovy, 1987: *Middle Atmospheric Dynamics*. Academic Press, 489 pp..

Beckmann, A., C. W. Böning, C. Köberle, and J. Willebrand, 1994: Effects of increased horizontal resolution in a simulation of the North Atlantic Ocean. *J. Phys. Oceanogr.*, **24**, 326–344..

Bleck, R., and D. B. Boudra, 1981: Initial testing of a numerical ocean circulation model using a hybrid (quasi-isopycnic) vertical coordinate. *J. Phys. Oceanogr.*, **11**, 755–770..

—, and —, 1986: Wind driven spin-up in eddy-resolving ocean models formulated in isopycnic and isobaric coordinates. *J. Geophys. Res.*, **91**, 7611–7621..

—, and L. T. Smith, 1990: A wind-driven isopycnic coordinate model of the north and equatorial Atlantic ocean. 1. Model development and supporting experiments. *J. Geophys. Res.*, **95**, 3273–3285..

—, H. P. Hanson, D. Hu, and E. B. Kraus, 1989: Mixed layer-thermocline interaction in a three-dimensional isopycnic coordinate model. *J. Phys. Oceanogr.*, **19**, 1417–1439..

Böning, C. W., 1989: Influences of a rough bottom topography on flow kinematics in an eddy-resolving circulation model. *J. Phys. Oceanogr.*, **19**, 77–97..

—, and R. C. Budich, 1992: Eddy dynamics in a primitive equation model: Sensitivity to horizontal resolution and friction. *J. Phys. Oceanogr.*, **22**, 361–381..

—, F. O. Bryan, R. Döscher, and W. R. Holland, 1996: Deep-water formation and meridional overturning in a high-resolution model of the North Atlantic. *J. Phys. Oceanogr.*, **26**, 1142–1164..

Bretherton, F. P., 1982: Ocean climate modeling. *Progress in Oceanography*, Vol. 11, Pergamon 93–129..

Bryan, K., 1986: Poleward buoyancy transport in the ocean and mesoscale eddies. *J. Phys. Oceanogr.*, **16**, 927–933..

—, 1991: Poleward heat transport in the ocean. *Tellus*, **43**, 104–115..

Carissimo, B. C., A. H. Oort, and T. H. Vonder Haar, 1985: Estimating the meridional energy transports in the atmosphere and ocean. *J. Phys. Oceanogr.*, **15**, 82–91..

Cox, M. D., 1985: An eddy-resolving numerical model of the ventilated thermocline. *J. Phys. Oceanogr.*, **15**, 1312–1324..

Danabasoglu, G., and J. C. McWilliams, 1995: Sensitivity of the global ocean circulation to parameterizations of mesoscale tracer transports. *J. Phys. Oceanogr.*, **25**, 2967–2987..

Davis, R. E., 1994: Diapycnal mixing in the ocean: Equations for large-scale budgets. *J. Phys. Oceanogr.*, **24**, 777–800..

Döös, K., and D. J. Webb, 1994: The Deacon cell and the other meridional cells of the Southern Ocean. *J. Phys. Oceanogr.*, **24**, 429–442..

Drijfhout, S. S., 1994a: On the heat transport by mesoscale eddies in an ocean circulation model. *J. Phys. Oceanogr.*, **24**, 353–369..

—, 1994b: Sensitivity of eddy-induced heat transport to diabatic forcing. *J. Geophys. Res.*, **99**, 18481–18499..

—, C. Heinze, M. Latif, and E. Maier-Reimer, 1996: Mean circulation and internal variability in an ocean primitive equation model. *J. Phys. Oceanogr.*, **26**, 559–580..

England, M. H., 1993: Representing the global-scale water masses in ocean general circulation models. *J. Phys. Oceanogr.*, **23**, 1523–1552..

Gent, P. R., and J. C. McWilliams, 1990: Isopycnic mixing in ocean circulation models. *J. Phys. Oceanogr.*, **20**, 150–155..

—, J. Willebrand, T. J. McDougall, and J. C. McWilliams, 1995: Parameterizing eddy-induced tracer transports in ocean circulation models. *J. Phys. Oceanogr.*, **25**, 463–474..

Hazeleger, W., and S. S. Drijfhout, 1998: Mode water variability in a model of the subtropical gyre: Response to anomalous forcing. *J. Phys. Oceanogr.*, **28**, 266–288..

Hirst, A. C., and T. J. McDougall, 1996: Deep-water properties and surface buoyancy flux as simulated by a Z-coordinate model including eddy-induced advection. *J. Phys. Oceanogr.*, **26**, 1320–1343..

Huang, R. X., and K. Bryan, 1987: A multilayer model of the thermohaline and wind-driven ocean circulation. *J. Phys. Oceanogr.*, **17**, 1909–1924..

Large, W. G., J. C. McWilliams, and S. C. Doney, 1994: Oceanic vertical mixing: A review and a model with a nonlocal boundary-layer parameterization. *Rev. Geophys.*, **32**, 363–403..

Lee, M.-M., and H. Leach, 1996: Eliassen–Palm flux and eddy potential vorticity flux for a nonquasigeostrophic time-mean flow. *J. Phys. Oceanogr.*, **26**, 1304–1319..

Luksch, U., 1996: Simulation of North Atlantic low-frequency SST variability. *J. Climate*, **9**, 2083–2092.. [Find this article online](#)

—, and H. von Storch, 1992: Modeling the low-frequency sea surface temperature variability in the North Pacific. *J. Climate*, **5**, 893–906.. [Find this article online](#)

Maier-Reimer, E., U. Mikolajewicz, and K. Hasselmann, 1993: Mean circulation of the Hamburg LSG OGCM and its sensitivity to the thermohaline surface forcing. *J. Phys. Oceanogr.*, **23**, 731–757..

McCann, M. P., A. J. Semtner, and R. M. Chervin, 1994: Transports and budgets of volume, heat, and salt from a global eddy-resolving ocean model. *Climate Dyn.*, **10**, 59–80..

Mikolajewicz, U., and E. Maier-Reimer, 1994: Mixed boundary conditions in OGCM's and their influence on the stability of the model's conveyor belt. *J. Geophys. Res.*, **99**, 22633–22644..

Oberhuber, J. M., 1993: Simulation of the Atlantic circulation with a coupled sea ice–mixed layer–isopycnal general circulation model. Part II: Model description. *J. Phys. Oceanogr.*, **23**, 808–829..

Polzin, K. L., J. M. Toole, J. R. Ledwell, and R. W. Schmitt, 1997: Spatial variability of turbulent mixing in the abyssal ocean. *Science*, **276**, 93–96..

Rahmstorf, S., and J. Willebrand, 1995: The role of temperature feedback in stabilising the thermohaline circulation. *J. Phys. Oceanogr.*, **25**, 787–805..

Sterl, A., and A. Kattenberg, 1994: Embedding a mixed layer model into an OGCM of the Atlantic: The importance of surface mixing for heat flux and temperature. *J. Geophys. Res.*, **99**, 14139–14157..

Stull, R. B., 1989: *An Introduction to Boundary Layer Meteorology*. Kluwer Academics, 666 pp..

Tandon, A., and C. Garrett, 1996: On a recent parameterization of mesoscale eddies. *J. Phys. Oceanogr.*, **26**, 406–411..

Wright, P. B., 1988: An atlas based on the COADS data set: Fields of mean wind, cloudiness and humidity at the surface of the global ocean. Max Planck Institute for Meteorology, Rep. 14, 70 pp. [Available from Max Planck Institute for Meteorology, Bundesstrasse 55, D-20146 Hamburg, Germany.]

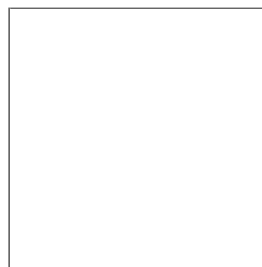
Tables

Table 1. Overview of the experiments.

Expt	Bottom topography	Linear coupling	Nonlinear coupling	Eddy resolving
1 ^a	x	x		
1 ^b	x	x		x
2 ^a	x			
2 ^b	x			x
3 ^a	x		x	
3 ^b	x		x	x
4 ^a		x		
4 ^b		x		x

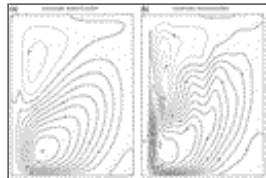
[Click on thumbnail for full-sized image.](#)

Figures



[Click on thumbnail for full-sized image.](#)

Fig. 1. Zonal wind stress and zonal apparent temperature used as forcing in the model. (Dotted line denotes summer; solid line denotes winter.)



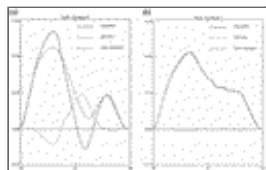
[Click on thumbnail for full-sized image.](#)

Fig. 2. Time-averaged barotropic streamfunction for experiment 1^a (left) and 1^b (right). Values are in Sverdrups ($10^6 \text{ m}^3 \text{ s}^{-1}$).



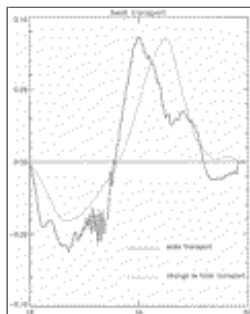
[Click on thumbnail for full-sized image.](#)

Fig. 3. Time-averaged mixed layer depth (in m) for experiment 1^b.



[Click on thumbnail for full-sized image.](#)

Fig. 4. Meridional heat transport in petawatts as a function of latitude (in degrees north), for experiment 1^a (left) and 1^b (right), including advective, diffusive, and total heat transport.



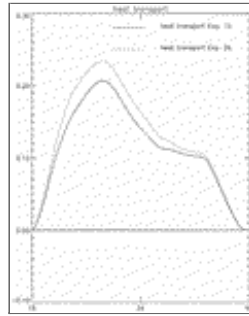
[Click on thumbnail for full-sized image.](#)

Fig. 5. Eddy heat transport and eddy-induced change in total heat transport for experiment 1^b.



[Click on thumbnail for full-sized image.](#)

Fig. 6. Thermal coupling coefficient in $\text{W m}^{-2} \text{K}^{-1}$ for experiment 1^b.



[Click on thumbnail for full-sized image.](#)

Fig. 7. Total meridional heat transport for experiments 1^b and 2^b.



[Click on thumbnail for full-sized image.](#)

Fig. 8. Time-averaged SST anomaly in degrees Celsius for experiment 1^b (relative to experiment 2^b).



[Click on thumbnail for full-sized image.](#)

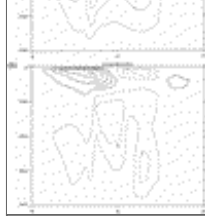
Fig. 9. Thermal coupling coefficient (in $\text{W m}^{-2} \text{K}^{-1}$) for experiment 3^b.



[Click on thumbnail for full-sized image.](#)

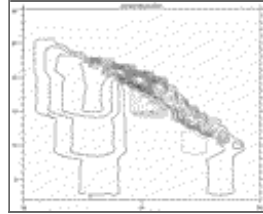
Fig. 10. Time-averaged barotropic streamfunction for experiment 4^b.





[Click on thumbnail for full-sized image.](#)

Fig. 11. Meridional mass transport as a function of depth and latitude for experiment 1^a (top) and 1^b (bottom). Values are in Sverdrups.



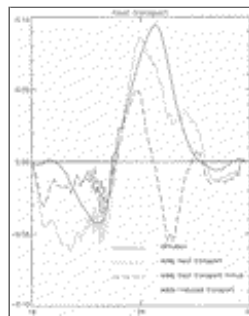
[Click on thumbnail for full-sized image.](#)

Fig. 12. Meridional mass transport as a function of potential temperature (density) for experiment 1^b.



[Click on thumbnail for full-sized image.](#)

Fig. 13. Eddy-induced change in meridional mass transport as a function of potential temperature (density) for experiment 1.



[Click on thumbnail for full-sized image.](#)

Fig. 14. Meridional heat transport in petawatts, including the diffusive transport in experiment 1^a, the eddy heat transport in 1^b, and the eddy heat transport minus eddy-induced change in total heat transport in experiment 1^b.

Corresponding author address: Dr. Sybren Drijfhout, Royal Netherlands Meteorological Institute, P.O. Box 201, 3730 AE De Bilt, the Netherlands.

E-mail: drijfhou@knmi.nl



© 2008 American Meteorological Society [Privacy Policy and Disclaimer](#)
Headquarters: 45 Beacon Street Boston, MA 02108-3693
DC Office: 1120 G Street, NW, Suite 800 Washington DC, 20005-3826
amsinfo@ametsoc.org Phone: 617-227-2425 Fax: 617-742-8718
[Allen Press, Inc.](#) assists in the online publication of *AMS* journals.